SNR G321.3–3.9 observed with multi-band radio data and SRG/eROSITA

A. Khokhriakova[1]   S. Mantovanini[2]   W. Becker[1,3]   N. Hurley-Walker[2]   G. E. Anderson[2]   L. Nicastro[4]

[1]Max-Planck-Institut für extraterrestrische Physik   [2]International Centre for Radio Astronomy Research, Curtin University

[3]Max-Planck-Institut für Radioastronomie   [4]INAF - Osservatorio di Astrofisica e Scienza dello Spazio di Bologna

Abstract

Detecting a supernova remnant (SNR) along the Galactic plane can be challenging. Any new detection reduces the discrepancy between the expected and known number of remnants. We present results from a large selection of radio and X-ray data that cover the position of G321.3–3.9. We identified G321.3–3.9 as a new SNR using data collected by several radio surveys spanning a frequency range from 200 to 2300 MHz. Stacked eROSITA data from four consecutive all-sky surveys (eRASS:4) provide spectro-imaging information in the energy band 0.2–8.0 keV.
G321.3–3.9 has an elliptical shape with major and minor axes of about $1.7° \times 1.1°$. From CHIPASS and S-PASS data, we calculate a spectral index $\alpha = -0.8 \pm 0.2$. The eROSITA data show an X-ray diffuse structure filling almost the entire radio shell. Based on our X-ray spectral analysis, we found the temperature to be approximately 0.6 keV and the column absorption density about 10^{21} cm^{-2}. Comparing this absorption density to optical extinction maps, we estimate the distance to fall within the range of (1.0–1.7) kpc, considering the 1σ uncertainty range.

arXiv:2401.17294

Radio data

Following the identification of the candidate in the Galactic Plane Monitoring (GPM) data, we searched all other archival surveys to detect this SNR candidate. We identified it in MGPS-2, CHIPASS, and S-PASS. It was also detected in the Rapid ASKAP Continuum Survey (RACS; McConnell et al. 2020) and the Evolutionary Map of the Universe (EMU, Norris et al. 2011), although the data was unsuitable for our analysis.

GPM Campaign
- Conducted from July to September 2022 with MWA.
- Covered 185–215 MHz, one-third of southern Galactic plane.
- Sensitivity: ∼1–2 mJy/beam; Angular resolution: 45″.
- Identified 21 SNR candidates, including G321.3–3.9.

MGPS-2 Survey
- Detection of G321.3–3.9 at 843 MHz.
- Conducted using Molonglo Observatory Synthesis Telescope (MOST).
- Remnant appears as a non-filled shell, brighter on the left.

CHIPASS Survey
- Covers sky south of declination $+25°$, central frequency 1394.5 MHz.
- Sensitivity: 40 mK.

S-PASS Survey
- Operates at 2303 MHz with a sensitivity of 9 mK.
- Covers entire southern sky below declination $-1°$.
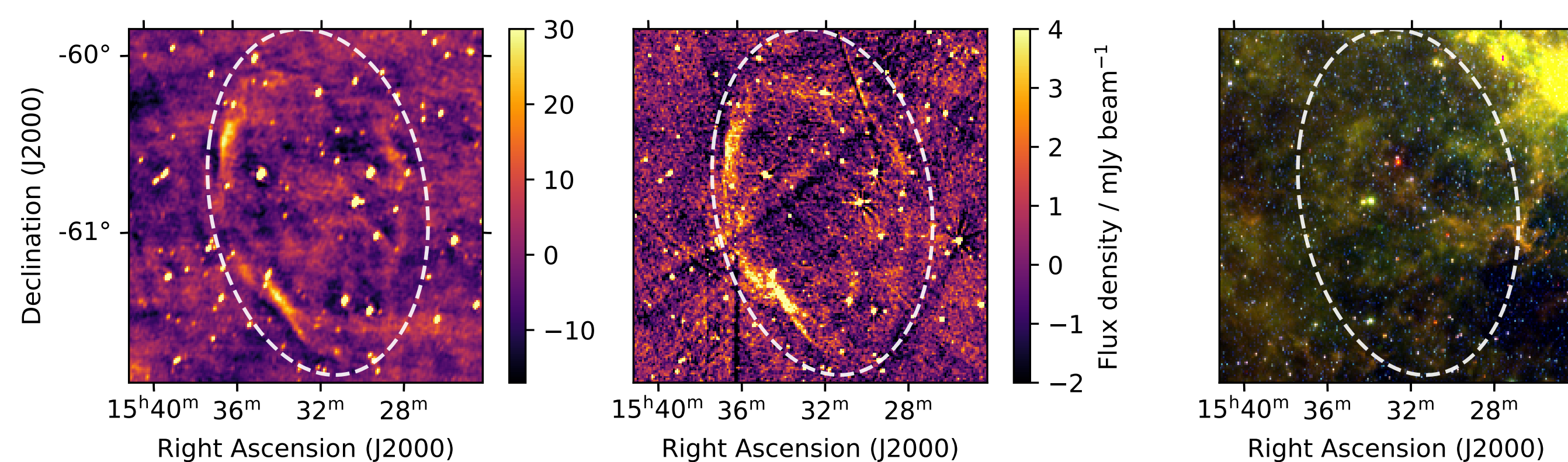- Detects polarized radio emission, providing magnetic field information.

Figure 1. $3.5° \times 3.5°$ region surrounding G321.3–3.9 as seen by GPM at 200 MHz in the left panel and by MGPS-2 at 843 MHz in the middle panel. Infrared zoomed-in visualization by WISE at 22 μm (R), 12 μm (G), and 3.4 μm (B) in the right panel. The white dashed line highlights the area the candidate is located in.

Radio spectral index

- We calculated the spectral index of G321.3–3.9 using the CHIPASS and S-PASS detections shown in Fig. 2. They were chosen because these single-dish measurements measure the total flux density of the source and do not "resolve out" the structure as is the case for interferometric measurements.
- We removed point sources within $2.3°$ of G321.3–3.9 and identified in MGPS-2 data.

Results
- CHIPASS (1400 MHz): 11.5 ± 0.6 Jy.
- S-PASS (2300 MHz): 7.6 ± 0.5 Jy.
- Spectral index $\alpha = -0.8 \pm 0.2$.

Expected spectral index range for SNRs: $-1.1 < \alpha < -0.1$ (Dubner and Giacani 2015).

Cross-check with WISE infrared data
- Absence of typical H II region morphology.
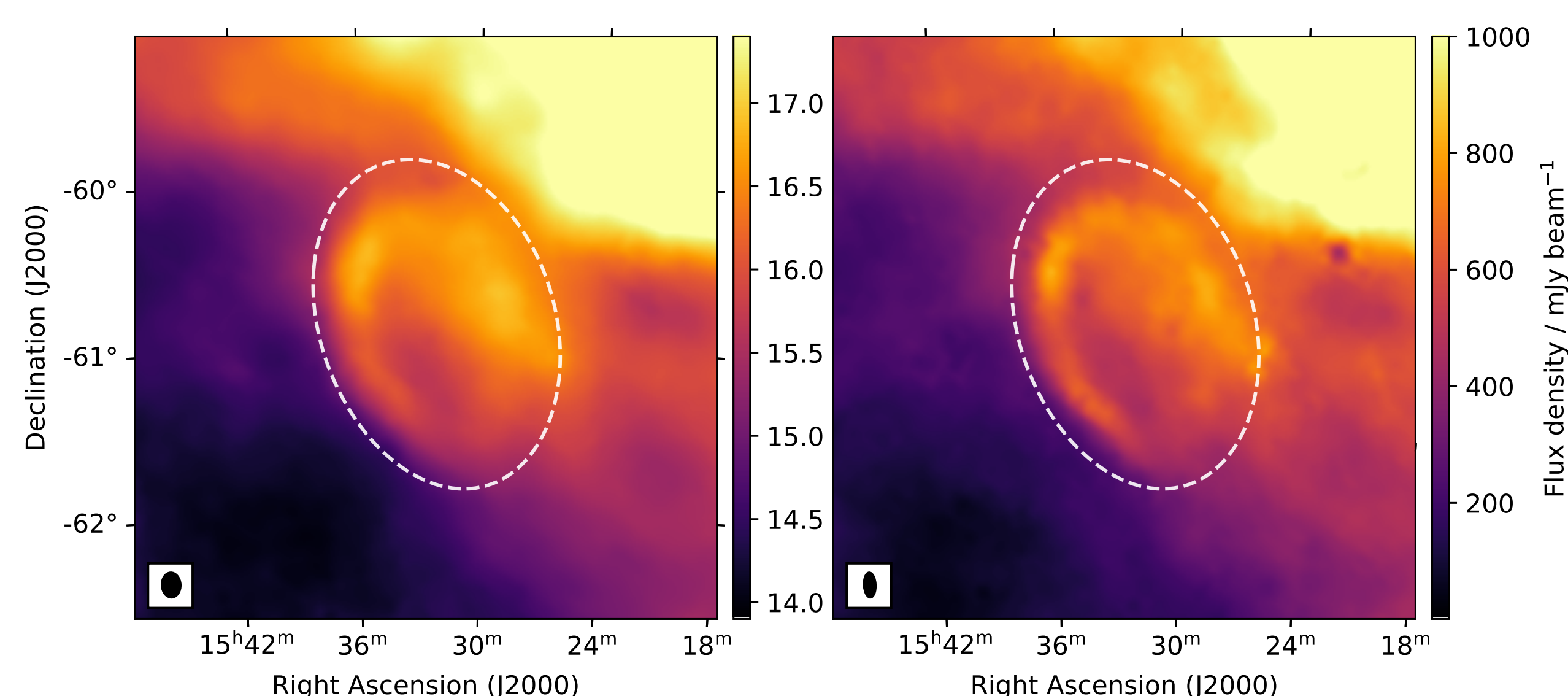- Radio emission confirmed as non-thermal.

Figure 2. $3.5° \times 3.5°$ of the region surrounding G321.3–3.9 as seen at 1.4 GHz by CHIPASS (left panel) and at 2.3 GHz by S-PASS (right panel). The panels show the region after the conversion from K to Jy beam^{-1} and the subtraction of point sources. The dashed line highlights the area within which the SNR is located.

eROSITA observations of G321.3–3.9

The eROSITA observations of G321.3–3.9 were conducted during the first four eROSITA all-sky surveys (eRASS:4) (Predehl et al. 2021; Sunyaev et al. 2021) in 2020 and 2021, resulting in an averaged exposure time of 710 seconds.
For image reconstruction, single-band images were created for energy bands 0.2–0.7 keV, 0.7–1.2 keV, and 1.2–8.0 keV, with no detection in the highest band. The adaptive kernel smoothing algorithm (Ebeling et al. 2006) was applied. Figure 3 shows the RGB composite image with the MWA radio image at 200 MHz used for the blue channel. The results show diffuse X-ray emission filling much of the remnant.
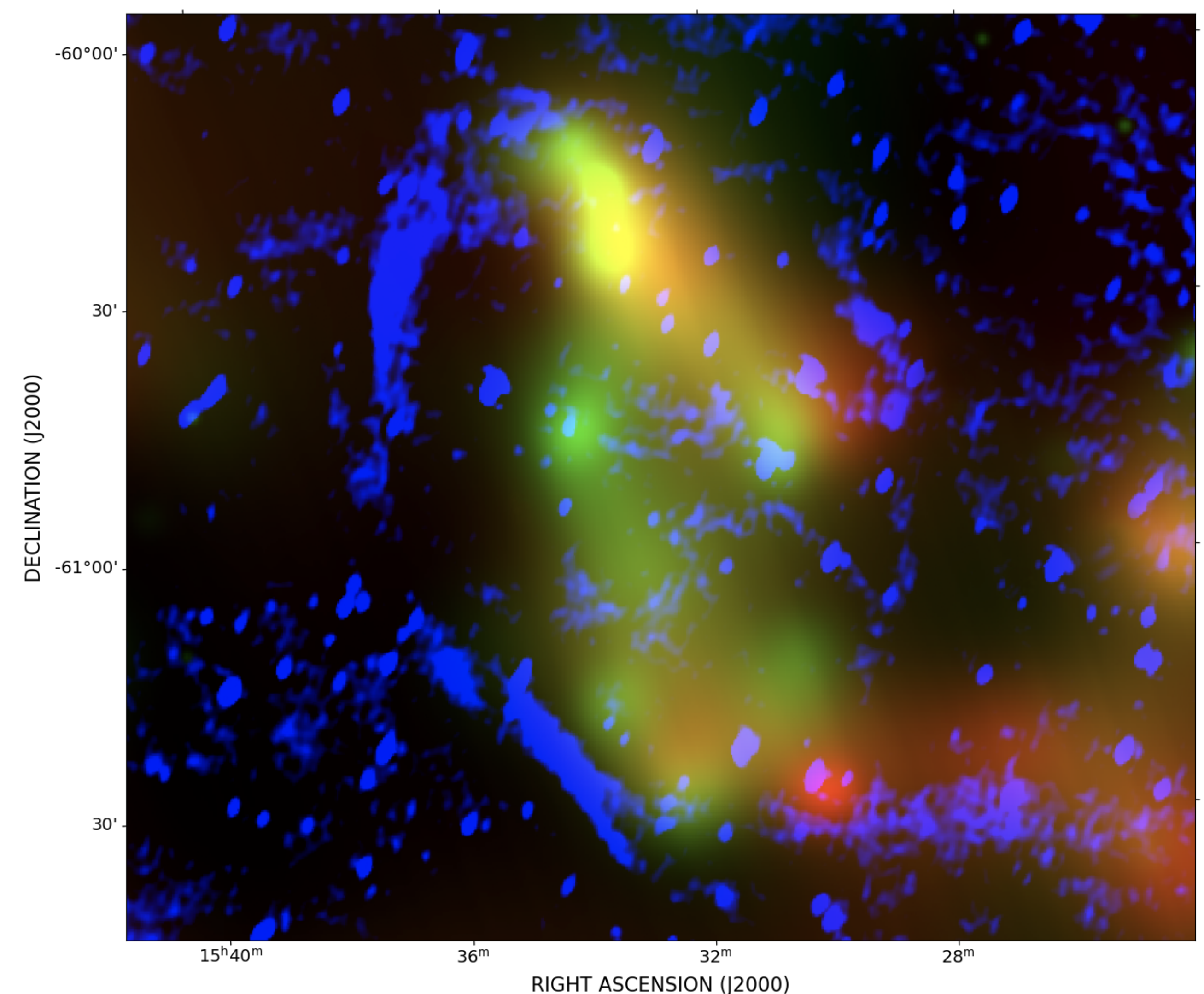

Figure 3. Composite RGB image of G321.3–3.9 as seen in the eROSITA all-sky surveys eRASS:4 and the MWA radio image taken at 200 MHz. X-ray photons to produce the image were color-coded according to their energy (red for energies 0.2–0.7, green for 0.7–1.2 keV), whereas the MWA image of G321.3–3.9 is shown in the blue channel.

X-ray spectral analysis

We conducted X-ray spectral analysis using PyXSPEC (Arnaud 1996), using eROSITA TMs 1–4 and 6 due to potential light leaks in TM5 and TM7. We used the Cash statistic (Cash 1979) and evaluated fit quality with the CSTAT/d.o.f. value. We removed point sources within the remnant's boundaries with a detection likelihood threshold of DETLIKE ≥ 70.
Our background model included instrumental background, absorbed extragalactic X-ray background, and a thermal component (Mayer et al. 2023). We tested three source spectral models: TBabs*vpshock, TBabs*vapec, and TBabs*vnei, allowing the abundances of O, Ne, Mg, Si, and Fe to vary.
The spectral models provided consistent temperatures around 0.6 keV and absorption column densities near 10^{21} cm^{-2}. Abundances had larger uncertainties, with noticeable scarcity of Ne and Mg. Fixing Ne and Mg to solar values resulted in less favorable fits, suggesting a thermonuclear supernova origin. The fitting results for all models are detailed in Table 1.

Table 1. Best fit parameters with 1σ errors obtained with different models, with O, Ne, Mg, Si, and Fe free to vary. All models include absorption (TBabs).

Model	vpshock	vapec	vnei
N_H (10^{22} cm^{-2})	$0.15^{+0.04}_{-0.03}$	$0.11^{+0.02}_{-0.02}$	$0.12^{+0.03}_{-0.02}$
kT (keV)	$0.65^{+0.03}_{-0.03}$	$0.58^{+0.02}_{-0.02}$	$0.58^{+0.02}_{-0.03}$
O/O$_\odot$	$0.17^{+0.08}_{-0.05}$	$0.18^{+0.15}_{-0.11}$	$0.08^{+0.08}_{-0.08}$
Ne/Ne$_\odot$	< 0.05	$0.3^{+0.18}_{-0.12}$	$0.17^{+0.08}_{-0.06}$
Mg/Mg$_\odot$	< 0.05	< 0.05	$0.06^{+0.09}_{-0.06}$
Si/Si$_\odot$	$0.6^{+0.2}_{-0.2}$	$0.51^{+0.14}_{-0.23}$	$0.6^{+0.3}_{-0.2}$
Fe/Fe$_\odot$	$0.5^{+0.2}_{-0.1}$	$0.30^{+0.07}_{-0.05}$	$0.37^{+0.09}_{-0.07}$
τ_u (10^{10} cm^{-3} s)	51^{+75}_{-26}	-	17^{+11}_{-4}
Normalization	$0.018^{+0.007}_{-0.005}$	$0.023^{+0.005}_{-0.005}$	$0.019^{+0.005}_{-0.004}$
Statistics	1756/1597=1.10	1794/1602=1.12	1790/1601=1.12

Normalization is expressed as $10^{-14}\frac{\int n_e n_H dV}{4\pi D^2}$ where n$_e$ is the electron density of the plasma (cm^{-3}), n$_H$ is the hydrogen density (cm^{-3}) and D (cm) is the distance of the source.